doi:10.1016/j.jmb.2007.07.039 J. Mol. Biol. (2007) 373, 112–126

JMB

Available online at www.sciencedirect.com
ScienceDirect

ELSEVIER

Structural Basis for Light-dependent Signaling in the Dimeric LOV Domain of the Photosensor YtvA

Andreas Möglich[1] and Keith Moffat[1,2]*

[1]*Department of Biochemistry and Molecular Biology, Institute for Biophysical Dynamics, University of Chicago, 929 East 57th Street GCIS W107A, Chicago IL 60637, USA*

[2]*Consortium for Advanced Radiation Sources (CARS), University of Chicago, 929 East 57th Street GCIS W107A, Chicago IL 60637, USA*

Received 4 May 2007; received in revised form 12 July 2007; accepted 17 July 2007
Available online 2 August 2007

Edited by R. Huber

The photosensor YtvA binds flavin mononucleotide and regulates the general stress reaction in *Bacillus subtilis* in response to blue light illumination. It belongs to the family of light-oxygen-voltage (LOV) proteins that were first described in plant phototropins and form a subgroup of the Per-Arnt-Sim (PAS) superfamily. Here, we report the three-dimensional structure of the LOV domain of YtvA in its dark and light states. The protein assumes the global fold common to all PAS domains and dimerizes *via* a hydrophobic interface. Directly C-terminal to the core of the LOV domain, an α-helix extends into the solvent. Light absorption causes formation of a covalent bond between a conserved cysteine residue and atom C(4a) of the FMN ring, which triggers rearrangements throughout the LOV domain. Concomitantly, in the dark and light structures, the two subunits of the dimeric protein rotate relative to each other by 5°. This small quaternary structural change is presumably a component of the mechanism by which the activity of YtvA is regulated in response to light. In terms of both structure and signaling mechanism, YtvA differs from plant phototropins and more closely resembles prokaryotic heme-binding PAS domains.

Keywords: light-oxygen-voltage; Per-Arnt-Sim; signal transduction; blue light sensor; YtvA

Introduction

Correct perception and integration of environmental signals are essential for the survival of all living organisms. Changes in external parameters such as light, redox potential or the concentrations of small molecules are frequently detected by sensor proteins such as members of the Per-Arnt-Sim (PAS) protein superfamily, which occur in all kingdoms of life.[1,2] Our research focuses on understanding the molecular mechanism of light-dependent signaling in proteins of the light-oxygen-voltage (LOV) family, which form a subgroup of the PAS family.[3,4] Through their flavin mononucleotide (FMN) cofactor, LOV photoreceptors absorb and react to blue light. LOV proteins from different organisms regulate the activity of numerous output or effector domains such as kinases, phosphodiesterases, zinc fingers and stress σ factors.[4,5] They were first identified in *Arabidopsis thaliana* phototropins, which control a variety of processes in plants, e.g. phototropism, chloroplast movement and stomatal opening.[3,6,7] In phototropins, two copies in tandem, LOV1 and LOV2, are linked to a Ser/Thr kinase domain. Whereas the LOV2 domain mediates light-dependent autophosphorylation and activation of phototropin, the role of the LOV1 domain is less clear.[8–10] Light-mediated activation of phototropin is not dependent on LOV1 photoactivity but requires LOV2 photoactivity.[11] The LOV1 domain appears to be involved in protein dimerization and to attenuate the light-mediated activation of phototropin by the LOV2 domain.[9,10,12]

Absorption of blue light initiates a photocycle during which a metastable covalent bond is formed between a conserved cysteine residue and atom C(4a) of the FMN ring.[13–15] High-resolution crystal structures of isolated phototropin LOV domains from *Adiantum capillus-veneris* (Japanese fern) and *Chlamydomonas reinhardtii* provide a molecular picture of the primary photoresponse following irradiation.[16–18] Light-induced structural changes were

**Corresponding author.* E-mail address: moffat@cars.uchicago.edu.

Abbreviations used: PAS, Per-Arnt-Sim; LOV, light-oxygen-voltage.

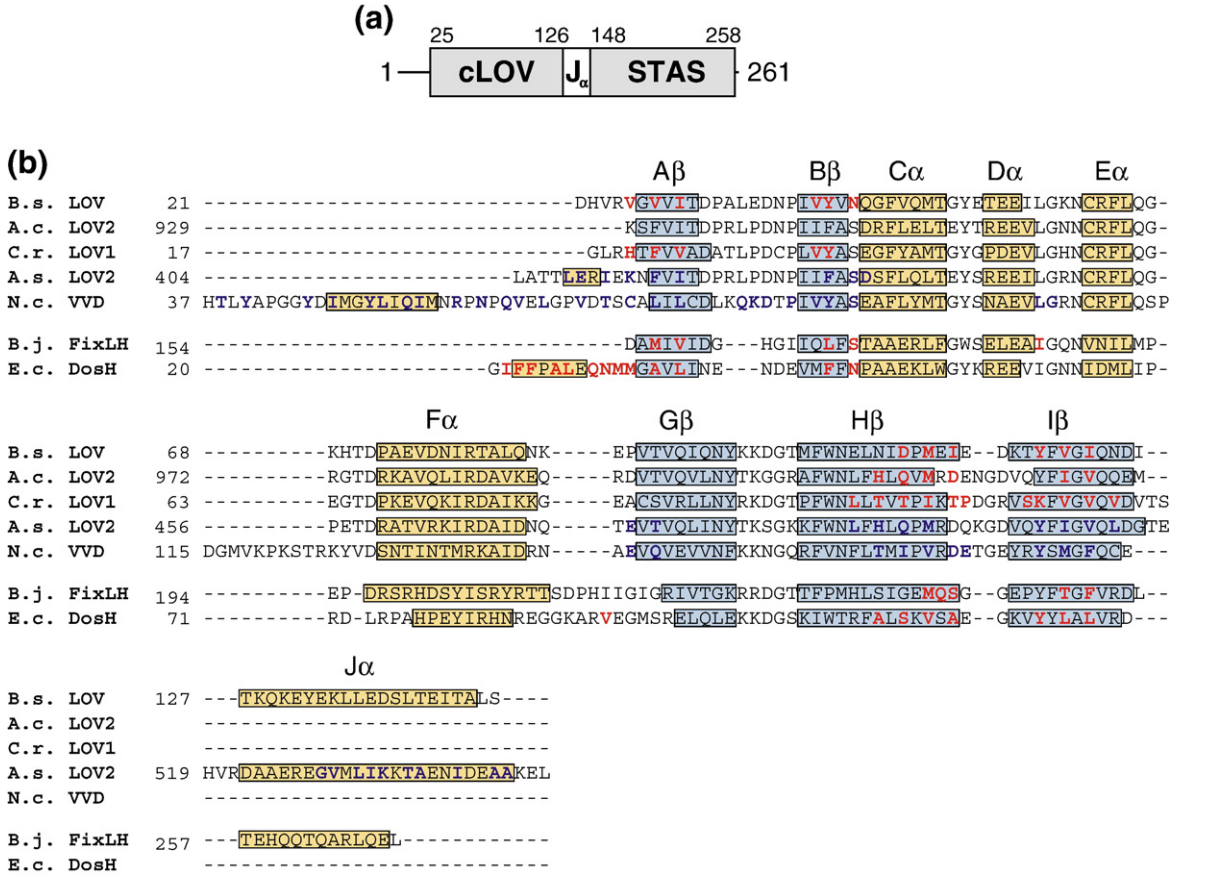

Figure 1. (a) Schematic of *B. subtilis* YtvA. The protein comprises an N-terminal extension (residues 1–24), a core LOV domain (cLOV, 25–126) and a STAS domain (148–258) joined by a short linker (Jα, 127–147). Domain boundaries have been assigned on the basis of sequence homology with known LOV and STAS structures. (b) Structure-based sequence alignment of YtvA-LOV from *B. subtilis* (B. s.) with LOV domains and heme-binding PAS domains of known three-dimensional structure. Secondary structure elements are indicated as shaded boxes, α-helices in yellow and β-strands in blue. Residues highlighted in bold red form homodimeric contacts in the crystal structure; residues in bold blue mediate intramolecular interactions between the core domain and C-terminal or N-terminal extensions. The sequence alignment shows only residues that were identified in the structures; amino acids introduced by cloning are not shown. Abbreviations denote phot1 LOV2 from *Avena sativa* (A. s., oat), phy3 LOV2 from *Adiantum capillus-veneris* (A. c., fern), phot1 LOV1 from *Chlamydomonas reinhardtii* (C. r.), Vivid from *Neurospora crassa* (N. c.), FixLH from *Bradyrhizobium japonicum* (B. j.) and *Escherichia coli* DosH (E. c.).

found to be small in extent, and largely confined to the immediate vicinity of the flavin ring. It remained unclear how the light signal is transmitted from the LOV domain to its conjugate effector domain. A new insight was provided by Gardner and co-workers, who studied a longer LOV2 construct from an *Avena sativa* (oat) phototropin and implicated an α-helical region, C-terminal to the core domain, in the signaling process. Upon absorption of blue light by the FMN cofactor, this helix, denoted Jα, unfolds, which is thought to facilitate signal propagation to the effector domain.[19,20] However, other work showed that the Jα helix may not be strictly necessary for kinase activation by LOV domains.[9]

To better understand the molecular basis for signaling in LOV proteins and to assess whether proteins from different species use a common signaling mechanism, we study the prokaryotic protein YtvA from *Bacillus subtilis*, which was first identified as a LOV photosensor based on sequence homology with plant phototropins.[21] It positively regulates the general stress transcription factor σ^B and is activated by blue light absorption.[22–24] Sequence comparison with LOV and STAS structures indicates that YtvA is composed of an N-terminal segment (residues 1–24), a core LOV domain (25–126) and a C-terminal sulfate transporter and anti-σ factor antagonist (STAS) domain (148–258) (Figure 1(a))†.[25] The core LOV and the STAS domains are connected by a linker region (127–147) that shows some sequence homology to the Jα helix in the structure of phot1 LOV2 from *Avena*.[19] The STAS domain was shown recently to bind trinucleotides.[26,27] In comparison to other FMN-binding LOV domains with known three-dimensional

†Core LOV domain refers to the protein region that comprises the canonical LOV/PAS domain fold, corresponding to residues 25–126 in YtvA.

Table 1. Pairwise sequence identity of LOV and heme-binding PAS domains of known three-dimensional structure

Sequence identity (%)	A.c. LOV2	C.r. LOV1	A.s. LOV2	N.c. VVD	B.j. FixLH	E.c. DosH
B.s. LOV	46	49	51	36	19	21
A.c. LOV2		48	73	38	15	21
C.r. LOV1			47	38	17	18
A.s. LOV2				41	17	21
N.c. VVD					19	20
B.j. FixLH						26

Sequence identities were calculated for the core LOV/PAS domains, corresponding to residues 25–126 in B. s. LOV, 929–1032 in A. c. LOV2, 20–123 in C. r. LOV1, 413–516 in A. s. LOV2, 71–185 in N. c. VVD, 154–256 in B. j. FixLH and 31–133 in E. c. DosH. Abbreviations are given in the legend to Figure 1.

structure, that from YtvA shows the slowest photocycle, with a recovery time after light absorption of the order of 1 h.[28]

We cloned, expressed and purified a protein construct comprising the core LOV domain of YtvA and the linker region (residues 20–147), referred to as YtvA-LOV in the following. Here, we report the crystal structures of YtvA-LOV in its dark (ground) state and in its light state‡. Distinct structural changes upon light absorption provide a molecular understanding of how light stimuli are detected and propagated within the LOV domain. On the basis of these data, we propose how the signal could be relayed to the STAS effector domain. Interestingly, in terms of both structure and signal transduction mechanism YtvA differs from plant phototropins and more closely resembles prokaryotic heme-binding PAS domains.

Results

Crystal structure of YtvA-LOV

Three-dimensional structures have been determined for the LOV2 domains from the fern *Adiantum capillus-veneris* phy3 (PDB 1G28, 1JNU)[16,17] and oat *Avena sativa* phot1 (NMR coordinates not deposited; A. Halavaty and K. M., unpublished results, PDB 2V0U, 2V0W),[19] and for LOV1 from *Chlamydomonas reinhardtii* phot1 (PDB 1N9L, 1N9O).[18] Very recently, the structure of the related FAD-binding LOV protein Vivid from *Neurospora crassa* was also determined (PDB 2PD7, 2PDR).[29] The core LOV domains (corresponding to residues 25–126 in YtvA) of these proteins and YtvA share between 36% and 73% identity in amino acid sequence (Table 1, Figure 1(b)).

Orthorhombic crystals of YtvA-LOV were grown in the dark and diffracted X-rays up to 1.45 Å resolution. Diffraction data were collected from a single crystal using synchrotron radiation, and the structure was solved by molecular replacement employing the dark state structure of the phot1 LOV1 domain from *C. reinhardtii* (PDB 1N9L) as the search model.[18] This LOV1 domain was chosen, since of all LOV structures with atomic coordinates available at that time, it shows the highest degree of sequence homology with YtvA (Table 1). The structure of YtvA-LOV was refined to an R_{work} of 19.0% and R_{free} of 22.4%. Detailed statistics of data collection and structure refinement are given in Table 2.

Within the asymmetric unit of the crystal, two molecules of YtvA-LOV related by a pseudo-dyad axis form a head-to-head dimer (Figure 2(a)). In monomers A and B, electron density could be resolved for residues 21–147 and 21–146. In both monomers, the core domains (residues 25–126) show the canonical fold previously observed for other LOV[4] and PAS[1,2] structures (Figure 1(b)), comprising a five-stranded antiparallel β-sheet (strands: Aβ residues 26–30, Bβ 39–42, Gβ 88–95, Hβ 101–113, Iβ 116–125) and four helices (Cα 44–50, Dα 54–56, Eα 62–65, Fα 72–83). A C-terminal helix (127–145), denoted Jα, does not form part of the core domain or pack against it. Rather, it points outwards and makes intermolecular contacts with the corre-

Table 2. Structural and refinement statistics of YtvA-LOV dark and light states

	Dark	Light
A. *Data collection*		
Max. resolution (Å)	1.45	1.95
Unit cell dimensions		
a (Å)	88.8	90.3
b (Å)	91.6	91.7
c (Å)	34.2	34.4
Total observations	316,788	162,761
Unique reflections	48728	21669
Resolution[a] (Å)	15.0–1.45 (1.49–1.45)	15.0–1.95 (1.98–1.95)
Redundancy[a]	6.6 (5.7)	7.5 (7.6)
Completeness[a] (%)	95.5 (99.9)	99.9 (99.8)
$I/\sigma(I)$[a]	36.3 (3.6)	26.4 (5.0)
R_{merge}[a] (%)	5.6 (44.9)	8.6 (37.1)
B. *Refinement*		
R_{work} (%)	19.0	18.1
R_{free} (%)	22.4	22.8
No. atoms	2637	2419
No. water moleculess	452	311
RMSD from ideal		
Bond lengths (Å)	0.008	0.016
Bond angles (deg.)	1.190	1.491
Ramachandran plot, residues in		
Most favored (%)	92.4	92.0
Additionally allowed (%)	7.6	7.6
Generously allowed (%)	0	0.4
PDB entry	2PR5	2PR6

For both states, the crystals had space group $P2_12_12$.
[a] Values in parentheses are for the highest resolution shell.

‡ Here, dark state refers to the protein in its equilibrium state in the absence of light. Light state designates the photostationary state of the protein obtained by illumination as described in Materials and Methods.

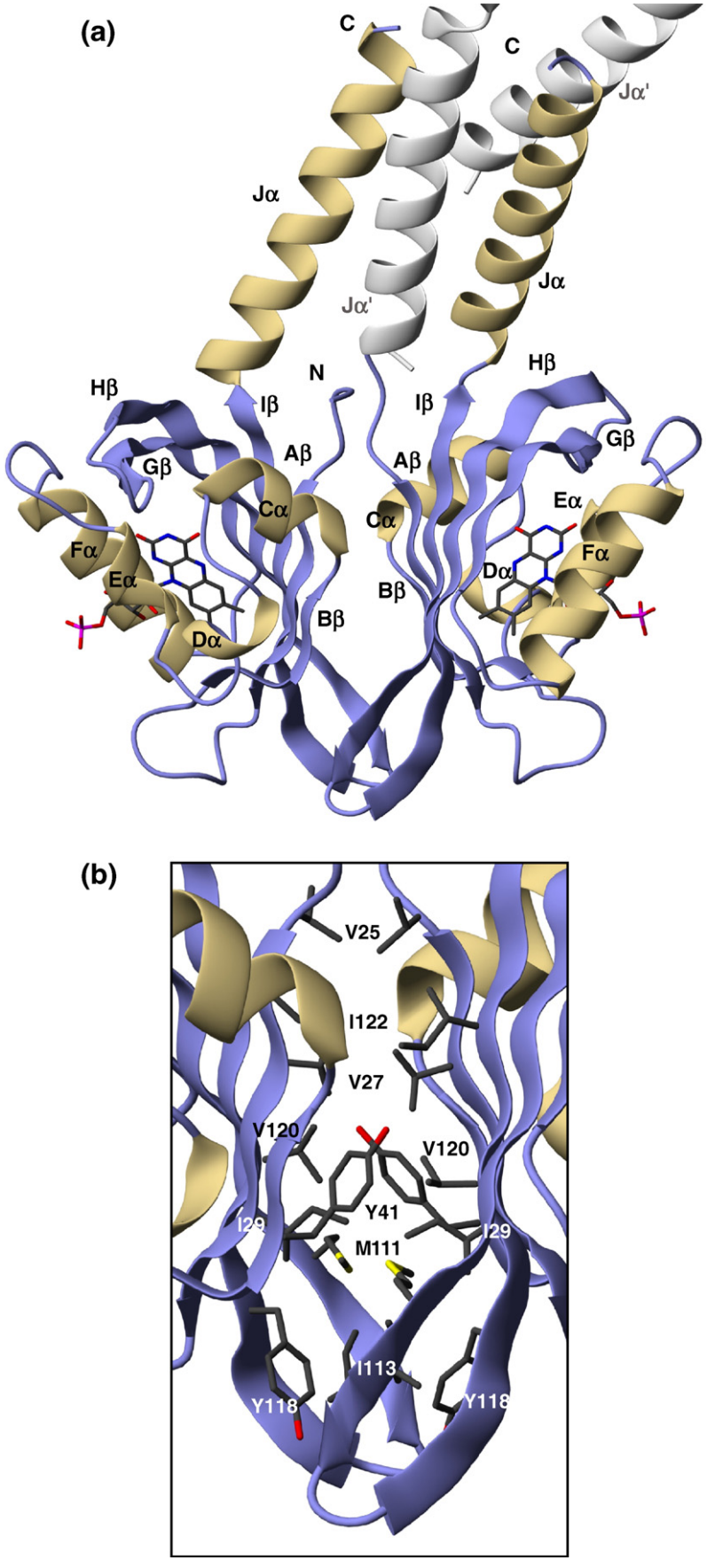

Figure 2. (a) Crystal structure of the head-to-head dimer of YtvA-LOV in its ground (dark) state. The FMN cofactors are highlighted in stick representation and the secondary structure elements (blue and light brown) are labeled. Within the crystal, the two C-terminal Jα helices form intermolecular contacts with the corresponding Jα′ helices of symmetry-related molecules (white). For clarity, only the Jα helices of symmetry-related molecules are shown. (b) The dimer interface. Hydrophobic residues V25, V27, I29, Y41, M111, I113, Y118, V120, and I122 located on the outside of the β-sheet in strands Aβ, Bβ, Hβ and Iβ form intermolecular contacts between the two monomers.

sponding Jα helices of symmetry-related molecules within the crystal. The orientation of the Jα helix relative to the core domain differs in the monomers A and B by 66°, probably due to crystal packing forces.

Superposition of the core domains (25–126) of monomers A and B yields an RMSD value of 0.48 Å for the backbone atom positions (Table 3). Structural differences between the two monomers are mainly confined to the AB, FG and HI loops. We compared YtvA-LOV with other known LOV structures and found RMSD values for the backbone atom positions of the core domain (25–126) that exceed 1 Å (Table 4). However, the main structural differences are concentrated in the HI loop. When this region (112–119) is excluded from the RMSD calculation, values between 0.5 Å and 0.7 Å are found, illustrating the close similarity in structure between these LOV domains. As judged by backbone RMSD values, YtvA-LOV most closely resembles the *Adiantum* LOV2 domain.[16]

The dimer interface of YtvA-LOV is formed by an extended network of hydrophobic residues across the pseudo-dyad axis and buries 1280 Å^2 of solvent-accessible surface area (Figure 2(b)). On the basis of this value, we estimate the free energy for dimerization to be −30 to −40 kJ mol^{-1}, corresponding to a dissociation constant between 5×10^{-6} and 7×10^{-8} M at 20 °C.[30] Residues contributing to the hydrophobic interface are located in strands Aβ (V25, V27, I29), Bβ (Y41), Hβ (M111, I113) and Iβ (Y118, V120, I122) of the β-sheet.

YtvA-LOV binds its cofactor FMN in a deep cleft formed primarily by residues located in the β-sheet and helices Eα and Fα (Figure 3(a)). The isoalloxazine ring is coordinated by a network of hydrogen bonds with the amide side-chains of Q66, N94, N104 and Q123, and by hydrophobic contacts with V28, T30, F46, L65, I78, L82, I92, L106 and I108. Two arginine residues, R63 and R79, form salt-bridges with the terminal phosphate group of FMN. The ribityl chain is stabilized by hydrogen bonds with N61, Q66 and two water molecules. As in the structure of phot1 LOV1 from *Chlamydomonas*,[18] two conformations for the side-chain of cysteine 62 with occupancies of 70% and 30% are observed. Comparison with other known LOV structures shows that the nature of the active site residues and their geometry is highly conserved between different species (Figure 3(b) and (c)). Differences are observed mainly in the coordination of the hydrophobic dimethyl benzene ring of FMN, whereas the network of polar and charged residues that coordinates the hydrophilic part of FMN is fully conserved.

Table 3. Comparison of YtvA-LOV dark and light state structures

Group 1	Group 2	RMSD (Å)
Dark, chain A	Dark, chain B	0.48
Light, chain A	Light, chain B	0.44
Dark, chain A	Light, chain A	0.24
Dark, chain B	Light, chain B	0.29
Dark, chains A and B	Light, chains A and B	0.36

RMSD values were calculated for the backbone atoms of residues 25–126.

Table 4. Pairwise backbone RMSD values of LOV domains of known three-dimensional structure

RMSD (Å)	B.s. LOV, chain A	A.c. LOV2, chain A	C.r. LOV1	A.s. LOV2[a]	N.c. VVD, chain A[b]
B.s. LOV, chain A	-	1.18	1.45	1.22	0.98
A.c. LOV2, chain A	0.55[c]	-	0.90	0.61	1.07
C.r. LOV1	0.66	0.75	-	0.93	1.35
A.s. LOV2[a]	0.60	0.44	0.80	-	1.07
N.c. VVD, chain A	0.67	0.63	0.82	0.68	-

RMSD values refer to backbone atom positions of the core LOV domains of the dark structures, corresponding to residues 25-126 in YtvA-LOV.

[a] A. Halavaty and K.M., unpublished results.

[b] For comparison with VVD, residues in the EF loop were excluded from the calculation (residues 113–127 in N. c. VVD).

[c] Values in the shaded boxes are calculated for backbone atom positions of residues 25–111 and 120–126.

YtvA-LOV is dimeric in solution

To determine the oligomeric state of YtvA-LOV in solution, we conducted sedimentation equilibrium experiments at concentrations of protein between 0.35 μM and 4.7 μM (Figure 4). Data obtained at all concentrations could be described globally by a single species of apparent molecular mass 34.5(±4.2) kDa, which reasonably corresponds to the expected molecular mass of 31.1 kDa for a dimer of YtvA-LOV. Even at the lowest experimentally accessible concentration of 0.35 μM, monomeric YtvA-LOV did not accumulate to any detectable extent. This provides an upper limit of approximately 2×10^{-7} M for the dissociation constant, K_D, of the monomer–dimer equilibrium under the conditions investigated. Our results agree qualitatively with those of Buttani *et al.*,[31] who reported the LOV domain of YtvA to be dimeric on the basis of gel-filtration chromatography.

We determined whether light absorption leads to structural changes. CD spectroscopy indicated that light absorption decreases the α-helical content of YtvA-LOV by approximately 10% (data not shown), which agrees with previous observations.[32] Although it is difficult to quantitatively evaluate CD spectra, these data indicate that light absorption does not lead to global unfolding or to pronounced loss of secondary structure elements. Light does not cause a significant change of oligomerization state in solution as assessed by fluorescence anisotropy measurements (data not shown). However, since these measurements were conducted at micromolar concentrations, we cannot rule out a possible effect of light on K_D that would be detectable only at lower concentrations.

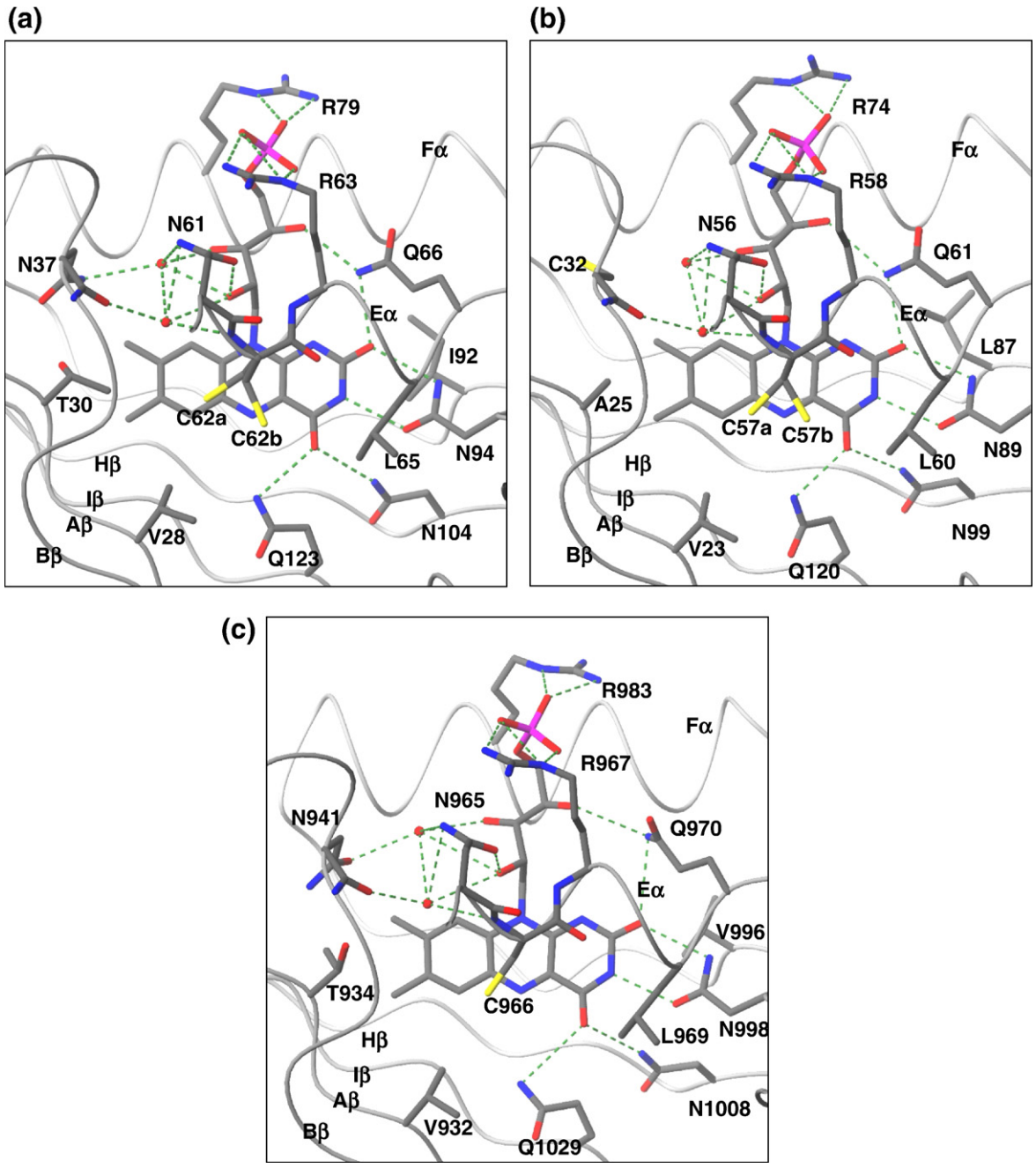

Figure 3. Comparison of the FMN-binding site in the dark state structures of (a) YtvA-LOV, (b) *Chlamydomonas* phot1 LOV1 and (c) *Adiantum* phy3 LOV2. Carbon atoms are shown in black, nitrogen atoms in blue, oxygen atoms in red, sulfur in yellow and phosphorus in magenta. Water molecules are depicted as red spheres. Broken green lines indicate hydrogen bonds or salt-bridges. The hydrogen bond network coordinating the FMN ring is highly conserved between the various LOV domains, whereas there is some variability in the hydrophobic residues lining the flavin ring. The key cysteine residue may adopt two conformations in the dark state, denoted a and b.

Structure of YtvA-LOV in its light state

To observe the structural changes effected within YtvA-LOV by light absorption, we determined its three-dimensional structure in the light-activated state. First, we tested whether YtvA-LOV is photoactive within the crystal. Single crystal microspectrophotometry allowed us to monitor absorption changes of the FMN cofactor following illumination, and revealed that YtvA-LOV undergoes a reversible photoreaction within the crystal corresponding directly to that observed in solution, albeit with a slightly shorter photorecovery time of 2000(±400) s compared to 3880(±20) s in solution at pH 7.0 and 23 °C (Supplementary Data Figure S1). In the crystallizing solution, the time constant for photorecovery is 3150(±20) s. Both in solution and in the crystal, the photorecovery process can be fully described by a single-exponential process (goodness of fit $R^2 > 0.99$); introduction of additional terms does

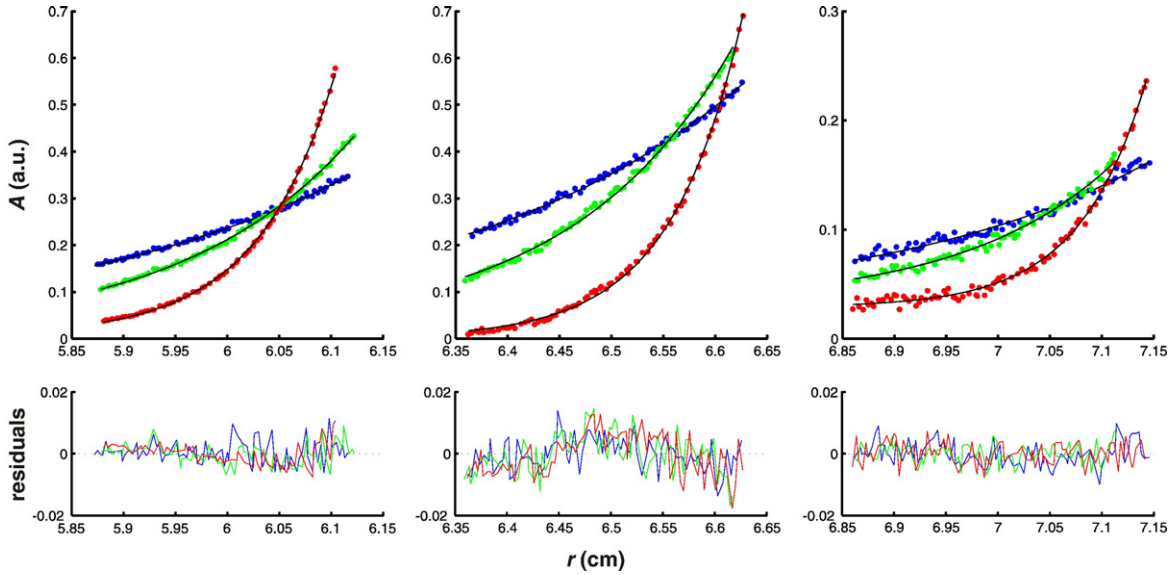

Figure 4. Sedimentation equilibrium centrifugation of YtvA-LOV. From left to right, protein concentrations are 4.7 μM, 1.3 μM and 0.35 μM. Experiments were conducted at 12,000 rpm (●), 16,000 rpm (●) and 24,000 rpm (●). The black lines represent a global fit of the data to a single species of apparent molecular mass 34.5(±4.2) kDa.

not improve the fit significantly. Thus, neither crystallization solution nor the additional intermolecular constraints present in the crystal lattice have a significant effect on the photorecovery time; and the photochemical properties of monomers A and B are closely similar.

These measurements also established conditions under which the light-activated state is predominantly populated in the crystal. Crystals of YtvA-LOV grown in the dark were illuminated accordingly and then cryo-cooled to 77K. Light-activated crystals diffracted X-rays to 1.95 Å, and allowed us to elucidate the structure of the protein in its light state. The structure was refined to an R_{work} of 18.1% and R_{free} of 22.8%. Refinement and structural statistics are given in Table 2.

Electron density could be resolved for residues 20–147 and 20–144 of monomers A and B. Overall, the three-dimensional structures of the dark and light states of YtvA-LOV share the same global fold. The RMSD values between the dark and light states for the backbone atom positions of the core domain (25–126) amount to 0.24 Å and 0.29 Å for monomers A and B, respectively (Table 3). For the dimeric complex, a corresponding RMSD value of 0.36 Å is obtained. It is noteworthy that the structural differences between dark and light states are qualitatively the same in both monomers despite their different crystallographic environments. Electron density maps indicate formation of a thioether bond between atoms S^{γ} of residue C62 and C(4a) of the FMN ring (Figure 5; Supplementary Data Figure S2). In the approximately 1–2 min that elapsed between illumination and cryo-cooling of YtvA-LOV crystals, about 3–6% of the molecules are expected to have reverted to their ground state. However, we can account for the diffraction data by assuming only one conformation for the active site cysteine. On the basis of these considerations, we estimate that the light-activated state of YtvA-LOV is populated to greater than 90% in the illuminated crystals. Formation of the thioether bond causes the flavin ring system to tilt by 6° towards C62, thus moving away from the dimer interface. Amino acid residues lining the FMN-binding pocket undergo slight displacements to accommodate this movement (Figures 5 and 6(a)). Q123, which in the dark state was proposed to form a hydrogen bond with atom O4 of the FMN ring,[16,18] undergoes a rearrangement, presumably involving a flip of its side-chain to form a hydrogen bond with the newly protonated N5 atom of the flavin ring.[17,18] However, the resolution of our diffraction data is too limited to resolve the orientation of the side-chain unambiguously in either the dark or the light state. Apart from Q123, geometry and distances of hydrogen bonds between the isoalloxazine ring and amide side-chains are largely maintained between the dark state and the light state (Figure 6(a)). Consequently, such residues, most notably N94 and N104, follow the light-induced movement of the FMN ring. In contrast, residues interacting with the dimethylbenzene moiety of FMN display only small changes between the dark and light states, for two possible reasons. On the one hand, interactions in this region are predominantly hydrophobic and thus non-directional; on the other hand, residues such as L106, I108, and F119 are located mainly in parts of the central β-sheet that are involved in dimerization and thus might not readily allow conformational rearrangements. Figure 6(b) illustrates how light-induced structural changes are further propagated from the FMN ring throughout the protein. The most profound movement is observed for F46, whose phenyl ring rotates by 70°, thereby filling space that was occupied by Q123 in the dark state. Residues L65 and I92 are adjacent to N94, N104, and the FMN ring, and follow their displacement away

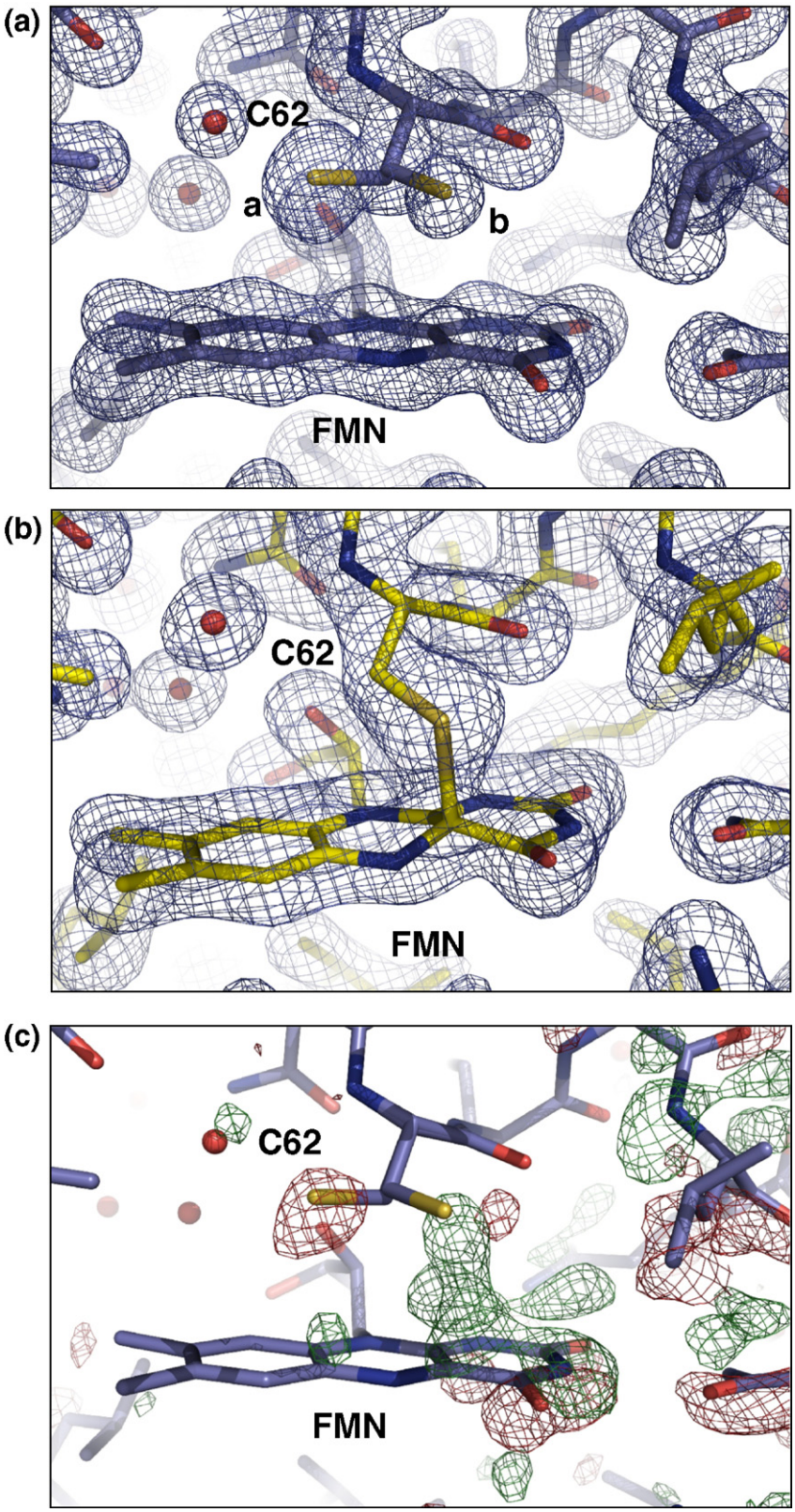

Figure 5. Electron density maps of the FMN-binding pocket in the dark and light states of YtvA-LOV. (a) The $2F_o$–F_c map of the dark state structure contoured at 1.0 σ. Note two conformations, a and b, for the active site cysteine 62. (b) The $2F_o$–F_c map of the light state structure contoured at 1.0 σ. Note formation of a covalent bond between S^{γ} of C62 and C(4a) of FMN. In comparison with the dark state, the plane of the isoalloxazine ring is tilted by 6°, which slightly displaces amino acids lining the binding pocket. (c) The difference electron density map F_{light}–F_{dark} contoured at ±2.5 σ. Positive density is shown in green, negative density is shown in red.

from the pseudo-dyad axis. Concomitantly, the entire protein region in which these residues are located, comprising strands Gβ and Hβ, helix Eα and the EF loop, bends away from the dimer interface. This also leads to a repositioning of amino acids on the outer face of the β -sheet and in the corresponding loop regions. Residues K68, H69, T89, Q91, Q93, Y95, M101, W103, and E105 are displaced towards the exterior of the protein. Residues I126, T127, and Q129 are located in the Jα helix and form contacts with strands Hβ and Iβ of the core domain. Through these interactions, light-induced structural changes are propagated to the Jα helix and cause it to swing away from the dimer

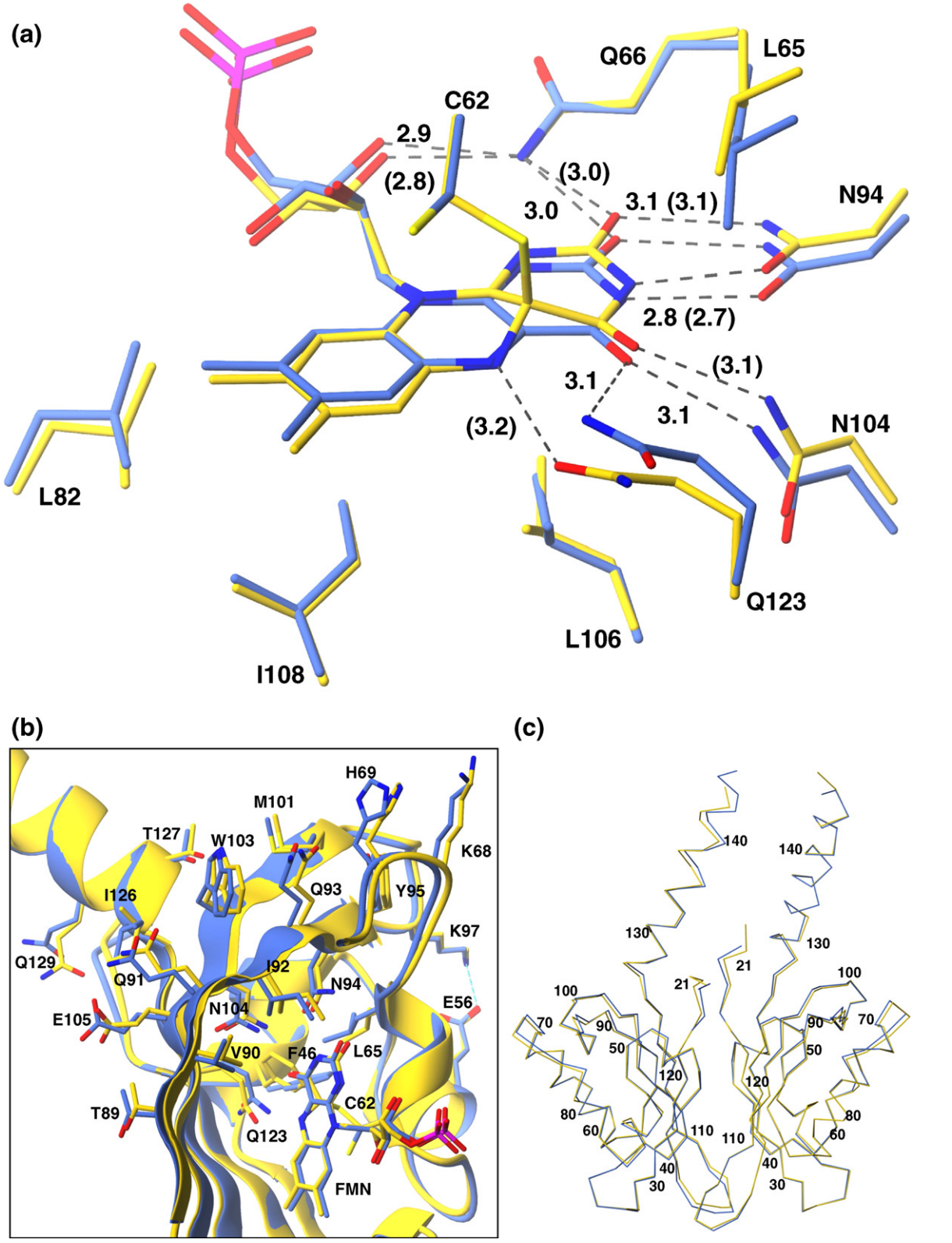

Figure 6. (a) Comparison of the FMN-binding pocket of YtvA-LOV in the dark (blue) and light (gold) states. Hydrogen bonds are indicated by broken lines; numbers give their length in Å. Values for the light state are shown in parentheses. Significant light-induced structural changes are observed mainly in the vicinity of the pyrimidine moiety of FMN. (b) Light-induced changes are propagated from the FMN-binding pocket to the outside of the molecule, mainly in the region of the EF loop, the GH hairpin and the Eα helix (see the text). Side-chains are depicted only for residues that undergo significant light-induced changes. For clarity, only one monomer of each structure is shown and helix Fα has been removed. (c) C^{α} traces of dark (blue) and light states (gold) of YtvA-LOV show that structural changes are the same in both monomers and occur mainly in the EF loop, the GH hairpin and the Jα helix. Structures are in the orientation shown in Figure 2(a).

interface. Small structural changes are observed also in the HI hairpins, which move towards the dimer interface (Figure 6(c)).

Discussion

Light absorption results in rotation of the two YtvA-LOV monomers

Light-induced structural changes originating at the FMN ring lead to spatially extensive rearrangements of YtvA-LOV, though no individual atomic motion is large (Figure 7(a)). Light absorption causes the GH hairpin, the EF loop, and helices Eα and Jα (the top halves of each monomer in Figure 7(a)), to tilt slightly away from the dimer interface. Concomitantly, the HI hairpins move towards the dimer interface (bottom halves of each monomer in Figure 7(a)). Overall, these structural changes cause the two monomers to rotate relative to each other, resulting in a quaternary structure change that can be characterized as a scissor-like motion. We quantified the extent of this rotation by calculating the moment of inertia tensor for the two monomers in the dark and light states. On average, the principal axes tilt by approximately 2–3° each, leading to a rotation of the monomers by 4–5° relative to each other.

A salt-bridge that is conserved between different PAS domains may have an important functional role.[4] Interestingly, in YtvA-LOV this salt-bridge between E56 and K97 is located within the region that undergoes the most pronounced light-induced structural changes (Figure 6(b)). However, in contrast to their immediate surroundings, these two residues show only minor rearrangements. Thus, in YtvA-LOV this salt-bridge might act to stabilize the protein during its photocycle. Support for this notion comes from the observation that mutating E56 to Gln slows the photocycle by a factor of 2.[32] Recent findings indicate that in the *A. thaliana* phot1 LOV2 domain, the main role of the conserved salt-bridge is to stabilize the native protein structure, rather than to propagate the light stimulus to the phot1 effector domain.[10]

Potential influence of crystal packing

An important concern for any crystallographic study is whether the constraints imposed by crystal packing affect the structure or changes in structure. In the YtvA-LOV structure, the Jα helices form many intermolecular contacts with symmetry-related molecules, which could influence their structure and impede light-induced motions (Figure 2(a)). These contacts probably account for the different orientation of the Jα helices in the two monomers of YtvA-LOV. While we cannot rule out an effect of crystal packing forces on structural changes in the Jα helices, we are confident that these forces have, at most, a minor influence on the core LOV domain. Qualitatively, the same structural changes are seen

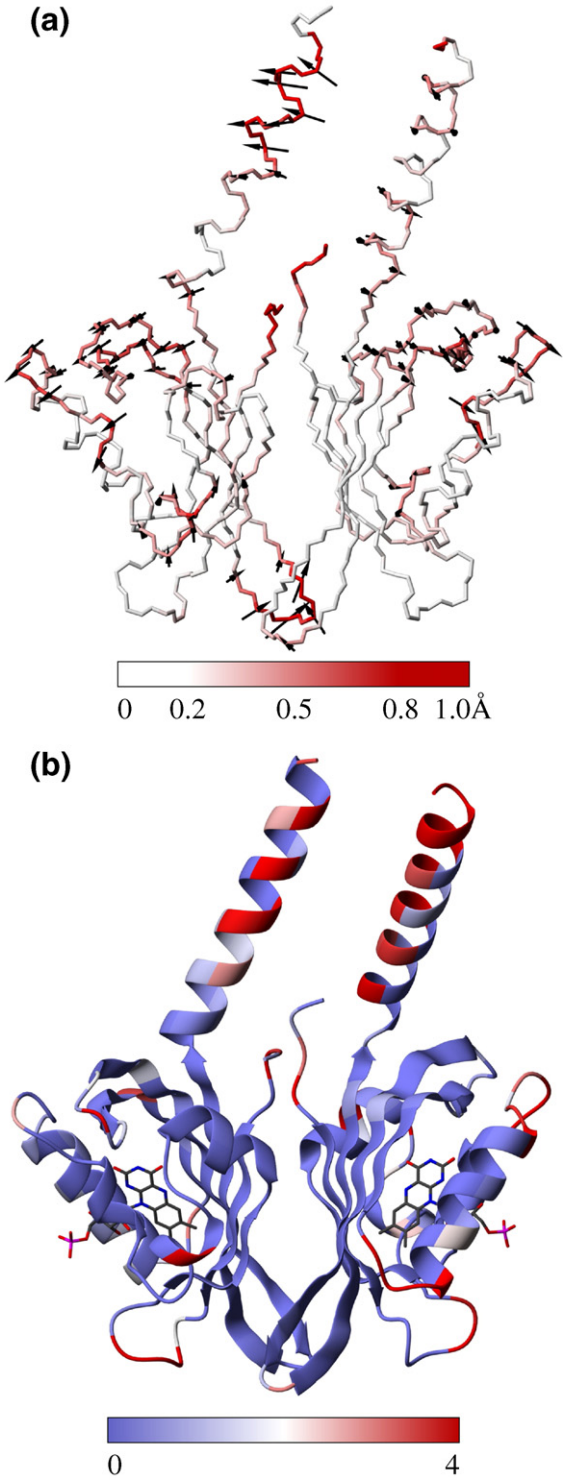

Figure 7. (a) Backbone trace of YtvA-LOV illustrating light-induced structural changes. Atoms are color-coded on the basis of their rms difference in position between dark and light structures. Black arrows indicate direction and magnitude of movements exceeding 0.4 Å. Structures are in the orientation shown in Figure 2(a). (b) Intermolecular contacts for YtvA-LOV in the crystal. Residues are color-coded on the basis of how many atoms from symmetry-related molecules are found within a 5 Å radius, normalized by the number of atoms in that residue. Note that, with the exception of the Jα helices and the AB loop, the two monomers make different contacts with symmetry mates. Structures are in the orientation shown in Figure 2(a).

in both subunits, although they differ considerably in their intermolecular contacts within the crystal (Figure 7(b)). Further, the crystallographic data largely agree with our solution experiments that show that light absorption does not cause global structural changes. However, as indicated by our CD measurements, in solution light absorption leads to approximately 10% loss of helical content, which would be compatible with partial, but not complete, unfolding of the Jα helices. The present structural data do not reveal which residues are responsible for the loss of helical signal. Potentially, light-induced conformational changes do not occur to full extent within the crystal. Alternatively, the loss of helical conformation might primarily involve protein regions that are not resolved in the X-ray structure.

In summary, we believe that our structural data capture the qualitative nature of the light-induced changes occurring in YtvA-LOV in solution, though the quantitative extent of these changes may be modified.

Differences in structure and signaling mechanism among LOV domains

While the core domain of YtvA-LOV (residues 25–126) adopts the same fold as other LOV domains, it differs considerably in quaternary structure and in the orientation of its C-terminal Jα helix. phot1 LOV2 from *Avena* is monomeric in its ground state and its Jα helix packs against the outer face of the central β-sheet[19] (A. Halavaty and K. M., unpublished results). phy3 LOV2 from *Adiantum* and phot1 LOV1 from *Chlamydomonas* were crystallized and studied as shorter constructs lacking their Jα helices.[16,18] Within the crystal, phy3 LOV2 formed a head-to-tail dimer by associating through its β-sheet. The *Chlamydomonas* LOV1 domain was found to be monomeric in solution and only one copy was found in the asymmetric unit of the crystal structure. Interestingly, within the crystal, this LOV domain forms a head-to-tail dimer with a symmetry-related molecule, which is reminiscent of the packing of the *Adiantum* LOV2 domain.

Although the overall level of sequence identity between these LOV domains is high (Table 1), they differ at crucial positions, which presumably account for the structural differences (Figure 1(b)). First, the hydrophobic patch on the surface of the β-sheet is more extended in YtvA than in the other proteins. The hydrophobic residue V25 at the beginning of strand Aβ in YtvA is replaced by charged or polar residues at this position in other LOV domains. Further, YtvA shows a deletion of two amino acids in the HI loop and, consequently, strands Hβ and Iβ are extended and adopt a conformation different from the other proteins. Second, as noted by Losi *et al.*,[32,33] the Jα helix in YtvA is connected to the core domain by only a short loop and overall has a more polar character than in other LOV domains. Thus, the Jα helix cannot readily bend and pack against the core domain. Consequently, the patch of hydrophobic residues on the outer face of the β-sheet is exposed and able to promote dimerization of YtvA-LOV (Figure 1(b)).

LOV domains also differ in their response towards light. In the *Avena* LOV2 domain, structural changes are transmitted from the FMN ring towards the β-sheet, culminating in the unfolding of the Jα helix. On the other hand, the proteins from *Adiantum* and *Chlamydomonas* were studied as shorter constructs that completely or partly lacked the residues of the Jα helix. Only minor conformational changes, primarily within the FMN-binding pocket, were observed. In the *Adiantum* LOV domain, small structural changes are also propagated to the CD and EF loops. Despite these differences, the active site geometry and the primary photoreaction, i.e. formation of a covalent bond between the FMN ring and the conserved cysteine residue, are remarkably similar between the various proteins (Figure 3). What, then, is the basis for the different photoresponses?

The extent and direction of light-induced structural changes within the various LOV domains are determined by the net balance of several forces acting upon the constituent atoms. On the one hand, light-induced formation of the thioether bond to FMN imposes stress on the LOV domain, which could be relieved by conformational rearrangements. On the other hand, elastic or restoring forces within the protein counteract such movements. The resultant observable light-induced structural changes arise from a combination of these two factors. Molecular dynamics simulations based on structural data on LOV domains could provide a more detailed understanding of these processes. Since, as detailed above, the primary photoreaction is essentially identical in the different LOV domains, structural properties may play the dominant role in governing the different photoresponses.

In both the *Adiantum* phy3 and YtvA-LOV domains, the central β-sheet is directly involved in forming extensive dimer contacts. Therefore, this region may not be able to undergo significant (light-induced) structural changes as in the *Avena* phot1 LOV2 domain. In contrast to YtvA-LOV, the *Adiantum* phy3 LOV2 domain possesses two salt-bridges between residues D948/R958 and R1004/E1031 that interconnect helix Cα with Dα and the GH loop with strand Iβ. These presumably confer additional stability on this protein region and might explain why light-induced structural changes in the fern protein are seen in a region adjacent to the corresponding one in YtvA-LOV. It is important to bear in mind that both the *Adiantum* and the *Chlamydomonas* LOV domains were crystallized as constructs lacking the C-terminal Jα helix, which might significantly affect the observable data. Furthermore, crystal packing forces could also influence the measurable data and partly account for the observed differences. However, in the crystal structures of the *B. subtilis* and the *Adiantum* LOV domains, several monomers with different packing contacts were found in the asymmetric units.[16] The

finding that the light-induced structural changes were the same in each subunit argues for only a minor influence of crystal packing.

Despite the structural differences, our data also provide new insight into the photoactivation mechanism of phototropin LOV domains. For the phot1 LOV2 domain from *Avena* it was shown that light absorption causes unfolding of the Jα helix, thus uncovering a hydrophobic patch on the outside of the central β-sheet.[19,34] Figure 1(b) illustrates that in different LOV domains structurally equivalent residues are involved in either forming a homodimeric complex or making intramolecular contacts to the C-terminal Jα helix. Therefore, exposure of hydrophobic residues in the β-sheet of the oat phot1 LOV2 domain upon light absorption could promote dimerization in a head-to-head fashion akin to the YtvA-LOV structure we report here. Indeed, recent work demonstrated light-induced dimerization of the homologous phot1 LOV2 domain from *A. thaliana*.[35] Dimerization of phototropin would facilitate autophosphorylation *in trans* and activation of the phot1 kinase domain.[8]

Recently, the dark and light structures of the FAD-binding LOV protein Vivid from *N. crassa* were reported.[29] Analogous to the *Avena* phot1 LOV2 domain, light absorption seems to cause unfolding or restructuring of a helical segment that extends from the core LOV domain at its N terminus. Interestingly, an N-terminal helical extension was also observed for the PAS domain of the redox sensor NifL from *Azotobacter vinelandii* and predicted to occur in certain other PAS domains.[36]

Structural and functional resemblance to prokaryotic heme-binding PAS domains

Of all known PAS domain structures, YtvA-LOV most closely resembles the bacterial oxygen sensor FixLH in its quaternary structure and the orientation of the C-terminal Jα helix.[37] This oxygen sensor domain binds heme as a cofactor and forms head-to-head dimers.[38] Furthermore, it possesses a C-terminal helix that extends from the protein core, much like the Jα helix in YtvA-LOV. However, conformational changes upon ligand binding occur in rather different regions of the PAS domain than in YtvA-LOV, and primarily involve the FG and HI loops.[38–40] It remains unclear how FixLH regulates the activity of its His kinase effector domain. Further, no functional role has yet been ascribed to the C-terminal helix in FixLH.

Although the protein construct of YtvA-LOV we studied did not include the STAS domain, our data suggest a possible mechanism for light regulation of the full-length YtvA protein. Light absorption causes the two monomers of YtvA-LOV to rotate apart by 4–5° (Figure 7(a)). Due to the extensive intermolecular contacts the Jα helices form in the crystal, it remains unclear how the signal is propagated to the effector domain. Possibly, the Jα helices would follow the rotational movement of the core domains and this could have a regulatory effect on the activity of the adjacent STAS domains. Apparently, the similarity to heme-binding PAS domains extends beyond the structural level, since a similar signaling mechanism was proposed earlier for the dimeric PAS redox sensor from *Escherichia coli* Dos (EcDos).[41,42] Although the mechanistic details differ, oxidation of a heme-coordinated iron leads to rotation of the two monomers relative to each other by 3°, which is thought to regulate the activity of the EcDos phosphodiesterase domain.

Conclusions

The high-resolution crystal structure of YtvA-LOV shows that the protein dimerizes in a head-to-head fashion. Light absorption leads to distinct structural changes within the LOV domain that are probably relevant for the regulation of the STAS domain. YtvA-LOV appears to use a signaling mechanism different from that proposed for plant phototropin LOV domains. Despite these differences, in YtvA-LOV, the C-terminal Jα helix also appears to play a pivotal role in signal transduction. Both in structural and mechanistic terms YtvA-LOV shows similarity to bacterial heme-containing PAS sensors. Structural and functional studies on the full-length YtvA protein are necessary to test the signaling mechanism we propose.

LOV and PAS domains represent remarkably versatile and malleable modules that have evolved to fulfil a variety of functions. Not only can they bind various ligands allowing the detection of several stimuli, but also they appear to employ a number of different yet recurring signaling pathways.

Materials and Methods

Cloning and purification of YtvA-LOV

The DNA sequence encoding residues 20–147 of YtvA was amplified from *B. subtilis* genomic DNA *via* PCR and cloned into the pET28c vector (Novagen, Madison, WI) using NdeI and SacI restriction sites to yield plasmid pAM001. Plasmid pAM001 had the correct sequence as confirmed by DNA sequencing and was transformed into *E. coli* BL21 (DE3) cells. Cells were grown to absorbance between 0.3 and 0.4 at 600 nm and protein expression was induced for 1 h at 37 °C in the dark by adding 1 mM isopropyl-β-d-thiogalactopyranoside. Cell lysis was carried out by sonication and the lysate was purified by metal ion affinity chromatography using Talon resin (Clontech, Mountain View, CA, USA). His_6-tagged protein was eluted from the resin with 200 mM imidazole and reconstituted with its cofactor FMN overnight at 4 °C. The His_6 affinity tag was cleaved by digesting with biotinylated thrombin (Novabiochem, San Diego, CA) for 2 h at 4 °C. Protease was removed quantitatively using streptavidin agarose and the protein was again passed over a Talon column. The protein was further purified *via* gel-filtration chromatography using Sephacryl 100 resin (Sigma, St. Louis, MO). Fractions containing YtvA-LOV were pooled and dialyzed against 10 mM Tris–HCl (pH 7.0), 10 mM NaCl. Dialyzed protein was concentrated

by spin filtration (Amicon Ultra, Millipore, Billerica, MA) to a final concentration of 10 mg/ml as determined by its absorbance using an extinction coefficient of 12,500 M^{-1} cm^{-1} at 450 nm.[32] Expression in the pET28 vector and thrombin cleavage introduced a four amino acid extension (GSHM) at the N terminus of the protein. All purification steps were carried out at 4 °C in the dark or under low levels of red light.

Crystallization and data collection

Crystal trays were set up under dim red light. Crystals of YtvA-LOV were grown in 3 μl hanging drops by vapor diffusion against buffer at 20 °C in the dark. Crystallization conditions were 5 mg/ml of protein, 0.1 M sodium acetate (pH 4.6), 18–22% (w/v) PEG-4000, 75–150 mM ammonium sulfate. Orthorhombic crystals of up to 0.3 mm × 0.25 mm × 0.15 mm in size appeared within three days. Crystals were mounted in CryoLoops (0.1–0.2 mm diameter, Hampton Research, Aliso Viejo, CA) and cryo-cooled within 1–2 min after opening the crystallization vessel. These procedures were carried out under low levels of red light. Cryo-cooled crystals were stored in the absence of light until data collection. X-ray diffraction data were collected at BioCARS beamline 14-BMC at the Advanced Photon Source, Argonne National Laboratory (Argonne, IL). Data were acquired in monochromatic oscillation mode at 100 K using a wavelength of 0.9 Å. Indexing, integration and scaling of diffraction spots were carried out using HKL2000.[43]

Structure determination

The structure was determined by molecular replacement using the program PHASER,[44] and the phot1 LOV1 domain from *C. reinhardtii* (PDB entry 1N9L) as search model.[18] The initial solution revealed two YtvA-LOV monomers in the asymmetric unit and had a crystallographic *R*-factor of 49.3%. Model building and refinement were carried out with Coot[45] and Refmac5,[46] respectively. The two YtvA-LOV monomers were refined independently. In the region of the N termini of both monomers, fragmentary electron density was observed that could not be fit reliably to protein residues. The final structure was obtained by TLS refinement.[47] Stereochemical quality was evaluated using PROCHECK.[48] Simulated annealing omit maps (Supplementary Data Figure S2) were calculated with CNS.[49] Coordinates for the FMN cofactor and atoms Cα, Cβ and S^{γ} of Cys62 were omitted from the structure model. Omit electron density maps were obtained by simulated annealing and *B*-factor refinement. For simulated annealing, the default parameters were used, corresponding to a slow cooling scheme from a starting temperature of 2500 K. Structure Figures were generated with MOLMOL,[50] Pymol§ and Povray‖.

Structure of the light state

Crystals of YtvA-LOV grown in the dark were illuminated at ambient temperature for 2 min using white light from a fiber optic illuminator (model 9745-00, Cole-Parmer Instrument Co., Chicago, IL). To prevent dehydration during light exposure, crystals were illuminated while still in their sealed crystallization vessel. Illuminated crystals were mounted as described above and cryo-cooled within 1–2 min after illumination. Further handling of crystals, X-ray data acquisition and processing were carried out as described above for the dark state. An initial solution for the light data set was obtained by using the phase information from the dark structure, and the structure was refined as detailed above.

Sequence alignment and structure comparison

Amino acid sequences of LOV and PAS domains were aligned on the basis of their three-dimensional structures using the program DaliLite.[51] Secondary structure elements were assigned based on the DSSP algorithm.[52] The alignment was manually edited in regions where secondary structure elements were not well matched. Intermolecular and intramolecular contacts shown in Figure 1(b) were evaluated using the PISA web server.[53] RMSD values and moment of inertia tensors were calculated with the program MOLMOL.[50] Intermolecular contacts within the crystal were evaluated with the program NCONT from the CCP4 suite.[54]

Analytical ultracentrifugation

Ultracentrifugation experiments were carried out on a Beckman Optima XL-A centrifuge (Palo Alto, CA) using a 60Ti rotor. Protein samples were diluted into 10 mM Tris–HCl (pH 7.0), 100 mM NaCl to concentrations of 0.35 μM, 1.3 μM and 4.7 μM. Sedimentation equilibrium runs were conducted in a six-sector cell at 20 °C and speeds of 12,000 rpm, 16,000 rpm and 24,000 rpm. Absorption data acquired at 215 nm, 230 nm and 280 nm were evaluated using MATLAB (MathWorks, Natick, MA). In the analysis, a value of 0.73 ml/g was used for the partial specific volume υ.[55] Confidence intervals of fitted parameters were determined by rigorous error analysis as described.[56] An upper limit for the dissociation constant K_D of the monomer–dimer equilibrium was estimated by simulating sedimentation equilibrium curves for different values of K_D.

Protein Data Bank accession codes

Atomic coordinates and structure factors for the dark and light structures of YtvA-LOV have been deposited in the Brookhaven Protein Data Bank under accession codes 2PR5 and 2PR6.

Acknowledgements

We gratefully acknowledge Emina Stojković for help with molecular biology, Xiaojing Yang and Andrei Halavaty for advice on crystallography, Vukica Šrajer for assistance with the microspectrophotometer measurements, and the staff at APS for help with data collection. Further, we thank Andrei Halavaty, Rebecca Ayers and other laboratory members for helpful discussions. Financial support by NIH grant GM036452 to K. M. is acknowledged. BioCARS is supported by NIH grant RR07707 to

§ http://pymol.sourceforge.net/
‖ http://www.povray.org

K. M.; the Advanced Photon Source is supported by the U.S. Department of Energy.

Supplementary Data

Supplementary data associated with this article can be found, in the online version, at doi:10.1016/j.jmb.2007.07.039

References

1. Taylor, B. L. & Zhulin, I. B. (1999). PAS domains: internal sensors of oxygen, redox potential, and light. *Microbiol. Mol. Biol. Rev.* **63**, 479–506.
2. Hefti, M. H., Francoijs, K. J., de Vries, S. C., Dixon, R. & Vervoort, J. (2004). The PAS fold. A redefinition of the PAS domain based upon structural prediction. *Eur. J. Biochem.* **271**, 1198–1208.
3. Huala, E., Oeller, P. W., Liscum, E., Han, I. S., Larsen, E. & Briggs, W. R. (1997). Arabidopsis NPH1: a protein kinase with a putative redox-sensing domain. *Science*, **278**, 2120–2123.
4. Crosson, S., Rajagopal, S. & Moffat, K. (2003). The LOV domain family: photoresponsive signaling modules coupled to diverse output domains. *Biochemistry*, **42**, 2–10.
5. Losi, A. (2004). The bacterial counterparts of plant phototropins. *Photochem Photobiol. Sci.* **3**, 566–574.
6. Briggs, W. R. & Christie, J. M. (2002). Phototropins 1 and 2: versatile plant blue-light receptors. *Trends Plant Sci.* **7**, 204–210.
7. Banerjee, R. & Batschauer, A. (2005). Plant blue-light receptors. *Planta*, **220**, 498–502.
8. Christie, J. M., Reymond, P., Powell, G. K., Bernasconi, P., Raibekas, A. A., Liscum, E. & Briggs, W. R. (1998). Arabidopsis NPH1: a flavoprotein with the properties of a photoreceptor for phototropism. *Science*, **282**, 1698–1701.
9. Matsuoka, D. & Tokutomi, S. (2005). Blue light-regulated molecular switch of Ser/Thr kinase in phototropin. *Proc. Natl Acad. Sci. USA*, **102**, 13337–13342.
10. Jones, M. A., Feeney, K. A., Kelly, S. M. & Christie, J. M. (2007). Mutational analysis of phototropin 1 provides insights into the mechanism underlying LOV2 signal transmission. *J. Biol. Chem.* **282**, 6405–6414.
11. Christie, J. M., Swartz, T. E., Bogomolni, R. A. & Briggs, W. R. (2002). Phototropin LOV domains exhibit distinct roles in regulating photoreceptor function. *Plant J.* **32**, 205–219.
12. Salomon, M., Lempert, U. & Rudiger, W. (2004). Dimerization of the plant photoreceptor phototropin is probably mediated by the LOV1 domain. *FEBS Letters*, **572**, 8–10.
13. Salomon, M., Christie, J. M., Knieb, E., Lempert, U. & Briggs, W. R. (2000). Photochemical and mutational analysis of the FMN-binding domains of the plant blue light receptor, phototropin. *Biochemistry*, **39**, 9401–9410.
14. Salomon, M., Eisenreich, W., Durr, H., Schleicher, E., Knieb, E., Massey, V. *et al.* (2001). An optomechanical transducer in the blue light receptor phototropin from Avena sativa. *Proc. Natl Acad. Sci. USA*, **98**, 12357–12361.
15. Swartz, T. E., Corchnoy, S. B., Christie, J. M., Lewis, J. W., Szundi, I., Briggs, W. R. & Bogomolni, R. A. (2001). The photocycle of a flavin-binding domain of the blue light photoreceptor phototropin. *J. Biol. Chem.* **276**, 36493–36500.
16. Crosson, S. & Moffat, K. (2001). Structure of a flavin-binding plant photoreceptor domain: insights into light-mediated signal transduction. *Proc. Natl Acad. Sci. USA*, **98**, 2995–3000.
17. Crosson, S. & Moffat, K. (2002). Photoexcited structure of a plant photoreceptor domain reveals a light-driven molecular switch. *Plant Cell*, **14**, 1067–1075.
18. Fedorov, R., Schlichting, I., Hartmann, E., Domratcheva, T., Fuhrmann, M. & Hegemann, P. (2003). Crystal structures and molecular mechanism of a light-induced signaling switch: the Phot-LOV1 domain from Chlamydomonas reinhardtii. *Biophys. J.* **84**, 2474–2482.
19. Harper, S. M., Neil, L. C. & Gardner, K. H. (2003). Structural basis of a phototropin light switch. *Science*, **301**, 1541–1544.
20. Harper, S. M., Christie, J. M. & Gardner, K. H. (2004). Disruption of the LOV-Jalpha helix interaction activates phototropin kinase activity. *Biochemistry*, **43**, 16184–16192.
21. Losi, A., Polverini, E., Quest, B. & Gärtner, W. (2002). First evidence for phototropin-related blue-light receptors in prokaryotes. *Biophys. J.* **82**, 2627–2634.
22. Akbar, S., Gaidenko, T. A., Kang, C. M., O'Reilly, M., Devine, K. M. & Price, C. W. (2001). New family of regulators in the environmental signaling pathway which activates the general stress transcription factor sigma(B) of Bacillus subtilis. *J. Bacteriol.* **183**, 1329–1338.
23. Gaidenko, T. A., Kim, T. J., Weigel, A. L., Brody, M. S. & Price, C. W. (2006). The blue-light receptor YtvA acts in the environmental stress signaling pathway of Bacillus subtilis. *J. Bacteriol.* **188**, 6387–6395.
24. Avila-Perez, M., Hellingwerf, K. J. & Kort, R. (2006). Blue light activates the sigmaB-dependent stress response of *Bacillus subtilis* via YtvA. *J. Bacteriol.* **188**, 6411–6414.
25. Aravind, L. & Koonin, E. V. (2000). The STAS domain—a link between anion transporters and antisigma-factor antagonists. *Curr. Biol.* **10**, R53–R55.
26. Buttani, V., Losi, A., Polverini, E. & Gärtner, W. (2006). Blue news: NTP binding properties of the blue-light sensitive YtvA protein from Bacillus subtilis. *FEBS Letters*, **580**, 3818–3822.
27. Buttani, V., Gärtner, W. & Losi, A. (2007). NTP-binding properties of the blue-light receptor YtvA and effects of the E105L mutation. *Eur. Biophys. J.* **36**, 831–839.
28. Losi, A., Quest, B. & Gärtner, W. (2003). Listening to the blue: the time-resolved thermodynamics of the bacterial blue-light receptor YtvA and its isolated LOV domain. *Photochem. Photobiol. Sci.* **2**, 759–766.
29. Zoltowski, B. D., Schwerdtfeger, C., Widom, J., Loros, J. J., Bilwes, A. M., Dunlap, J. C. & Crane, B. R. (2007). Conformational switching in the fungal light sensor Vivid. *Science*, **316**, 1054–1057.
30. Eisenberg, D. & McLachlan, A. D. (1986). Solvation energy in protein folding and binding. *Nature*, **319**, 199–203.
31. Buttani, V., Losi, A., Eggert, T., Krauss, U., Jaeger, K. E., Cao, Z. & Gärtner, W. (2007). Conformational analysis of the blue-light sensing protein YtvA reveals a competitive interface for LOV-LOV dimerization and interdomain interactions. *Photochem. Photobiol. Sci.* **6**, 41–49.
32. Losi, A., Ghiraldelli, E., Jansen, S. & Gärtner, W. (2005). Mutational effects on protein structural

changes and interdomain interactions in the blue-light sensing LOV protein YtvA. *Photochem. Photobiol.* **81**, 1145–1152.
33. Losi, A., Ternelli, E. & Gärtner, W. (2004). Tryptophan fluorescence in the Bacillus subtilis phototropin-related protein YtvA as a marker of interdomain interaction. *Photochem. Photobiol.* **80**, 150–153.
34. Corchnoy, S. B., Swartz, T. E., Lewis, J. W., Szundi, I., Briggs, W. R. & Bogomolni, R. A. (2003). Intramolecular proton transfers and structural changes during the photocycle of the LOV2 domain of phototropin 1. *J. Biol. Chem.* **278**, 724–731.
35. Nakasone, Y., Eitoku, T., Matsuoka, D., Tokutomi, S. & Terazima, M. (2006). Kinetic measurement of transient dimerization and dissociation reactions of Arabidopsis phototropin 1 LOV2 domain. *Biophys. J.* **91**, 645–653.
36. Key, J., Hefti, M., Purcell, E. B. & Moffat, K. (2007). Structure of the redox sensor domain of Azotobacter vinelandii NifL at atomic resolution: signaling, dimerization, and mechanism. *Biochemistry*, **46**, 3614–3623.
37. Gong, W., Hao, B., Mansy, S. S., Gonzalez, G., Gilles-Gonzalez, M. A. & Chan, M. K. (1998). Structure of a biological oxygen sensor: a new mechanism for heme-driven signal transduction. *Proc. Natl Acad. Sci. USA*, **95**, 15177–15182.
38. Key, J. & Moffat, K. (2005). Crystal structures of deoxy and CO-bound bjFixLH reveal details of ligand recognition and signaling. *Biochemistry*, **44**, 4627–4635.
39. Hao, B., Isaza, C., Arndt, J., Soltis, M. & Chan, M. K. (2002). Structure-based mechanism of O2 sensing and ligand discrimination by the FixL heme domain of Bradyrhizobium japonicum. *Biochemistry*, **41**, 12952–12958.
40. Key, J., Srajer, V., Pahl, R. & Moffat, K. (2007). Time-resolved crystallographic studies of the heme domain of the oxygen sensor fixl: structural dynamics of ligand rebinding and their relation to signal transduction. *Biochemistry*, **46**, 4706–4715.
41. Kurokawa, H., Lee, D. S., Watanabe, M., Sagami, I., Mikami, B., Raman, C. S. & Shimizu, T. (2004). A redox-controlled molecular switch revealed by the crystal structure of a bacterial heme PAS sensor. *J. Biol. Chem.* **279**, 20186–20193.
42. Park, H., Suquet, C., Satterlee, J. D. & Kang, C. (2004). Insights into signal transduction involving PAS domain oxygen-sensing heme proteins from the X-ray crystal structure of Escherichia coli Dos heme domain (Ec DosH). *Biochemistry*, **43**, 2738–2746.
43. Otwinowski, Z. & Minor, W. (1997). Processing of X-ray diffraction data collected in oscillation mode. *Methods Enzymol.* **276**, 307–326.
44. McCoy, A. J., Grosse-Kunstleve, R. W., Storoni, L. C. & Read, R. J. (2005). Likelihood-enhanced fast translation functions. *Acta Crystallog. sect. D*, **61**, 458–464.
45. Emsley, P. & Cowtan, K. (2004). Coot: model-building tools for molecular graphics. *Acta Crystallog. sect. D*, **60**, 2126–2132.
46. Murshudov, G. N., Vagin, A. A. & Dodson, E. J. (1997). Refinement of macromolecular structures by the maximum-likelihood method. *Acta Crystallog. sect. D*, **53**, 240–255.
47. Schomaker, V. & Trueblood, K. N. (1968). On the rigid-body motion of molecules in crystals. *Acta Crystallog. sect. B*, **24**, 63–76.
48. Laskowski, R. A., MacArthur, M. W., Moss, D. S. & Thornton, J. M. (1993). PROCHECK: a program to check the stereochemical quality of protein structures. *J. Appl. Crystallog.* **26**, 283–291.
49. Brünger, A. T., Adams, P. D., Clore, G. M., DeLano, W. L., Gros, P., Grosse-Kunstleve, R. W. *et al.* (1998). Crystallography & NMR system: a new software suite for macromolecular structure determination. *Acta Crystallog. sect. D*, **54**, 905–921.
50. Koradi, R., Billeter, M. & Wüthrich, K. (1996). MOLMOL: a program for display and analysis of macromolecular structures. *J. Mol. Graph.* **14**, 51–55.
51. Holm, L. & Sander, C. (1996). Mapping the protein universe. *Science*, **273**, 595–603.
52. Kabsch, W. & Sander, C. (1983). Dictionary of protein secondary structure: pattern recognition of hydrogen-bonded and geometrical features. *Biopolymers*, **22**, 2577–2637.
53. Krissinel, E. & Henrick, K. (2007). Inference of macromolecular assemblies from crystalline state. *J. Mol. Biol*. In the press (http://dx.doi.org/10.1016/j.jmb.2007.05.022).
54. Collaborative Computational Project Number 4. (1994). The CCP4 suite: programs for protein crystallography. *Acta Crystallog. sect. D*, **50**, 760–763.
55. Ralston, G. (1993). *Introduction to Analytical Ultracentrifugation.* Beckman Instruments, Fullerton, CA.
56. Bevington, P. R. & Robinson, D. K. (2003). *Data Reduction and Error Analysis for the Physical Sciences.* McGraw-Hill, New York.